Effect of *A*-site cation ordering on the magnetoelectric properties in $[(\text{LaMnO}_3)_m/(\text{SrMnO}_3)_m]_n$ artificial superlattices

T. Koida,[1] M. Lippmaa,[2,3] T. Fukumura,[4] K. Itaka,[1,3] Y. Matsumoto,[5] M. Kawasaki,[3,4,5] and H. Koinuma[1,3,5,6]

[1]*Frontier Collaborative Research Center, Tokyo Institute of Technology, 4259 Nagatsuta, Midori, Yokohama 226-8503, Japan*

[2]*Institute for Solid State Physics, University of Tokyo, Kashiwanoha, 5-1-5, Kashiwa, 277-8581, Japan*

[3]*Combinatorial Materials Exploration and Technology (COMET), 4259, Nagatsuta, Midori, Yokohama 226-8503, Japan*

[4]*Institute for Materials Research, University of Tohoku, 2-1-1, Katahira, Sendai, 980-8577, Japan*

[5]*Ceramics Materials and Structures Laboratory, Tokyo Institute of Technology, 4259, Nagatsuta, Midori, Yokohama 226-8503, Japan*

[6]*CREST, Japan Science and Technology Corporation, S-507, Bldg. 55, Waseda University, 3-4-1 Okubo, Shinjuku, 169-0072, Japan*

In order to evaluate the effect of charge transfer and/or charge ordering in $\text{La}_{1-x}\text{Sr}_x\text{MnO}_3$ on the magnetic and transport properties, a library of $[(\text{LaMnO}_3)_m/(\text{SrMnO}_3)_m]_n$ superlattices have been fabricated by the combinatorial pulsed laser deposition method. The properties of superlattices were found to depend strongly on the periodicity m; superlattices of $m \leq 4$ behaved like a solid solution $\text{La}_{0.5}\text{Sr}_{0.5}\text{MnO}_3$ film, while the superlattices of $m > 4$ were significantly different from the solid solution. These superlattices exhibited a higher resistivity and lower Curie temperature than $m \leq 4$ superlattices. The results indicate that the properties of the superlattices are dominated not only by the magnetic interaction between the superlattice constituents but also by carrier (e_g electrons) transfer thorough the superlattice interface. The contribution of carrier transfer is supported by the magnetoelectric properties of another library of $[(\text{La}_{0.8}\text{Sr}_{0.2}\text{MnO}_3)_8/(\text{La}_{0.2}\text{Sr}_{0.8}\text{MnO}_3)_m]_{12}$ superlattices. The *A*-site cation order can change both effective carrier concentration and magnetic interaction.

I. INTRODUCTION

The discovery of colossal magnetoresistance (CMR) attracted much interest to perovskite manganites $R_{1-x}A_x\text{MnO}_3$ (where R is a rare-earth ion and A an alkaline-earth ion). They show versatile magnetic and electrical properties as a function of the doping concentration (x) and their phase diagram has been mapped out through numerous experiments using bulk crystalline samples.[1] The phase diagram of $\text{La}_{1-x}\text{Sr}_x\text{MnO}_3$ was also mapped out by rapidly characterizing composition-spread films fabricated on a single substrate using the combinatorial pulsed laser deposition method. The good agreement between both methods verified the high efficiency of the combinatorial approach using a thin film library.[2] Generally, the origin of CMR is attributed to a double exchange mechanism[3] in which polaron formation originating from a Jahn-Teller instability[4] is involved. However, there are several experimental results hardly explained by this mechanism alone. The phase separation phenomenon is one of them. The coexistence of different magnetic phases[5–9] and electrical phases[10,11] has been observed in several $R_{1-x}A_x\text{MnO}_3$ bulk materials, often as the occurrence of CMR phenomena. The control of phase separation by temperature and doping levels would be an important parameter to govern the material properties.

The phase separation phenomena were investigated both theoretically and experimentally. The theoretical calculation indicates that the increase of charge fluctuation influences the ground state of the material and occasionally induces phase segregation.[12] Experimental studies using NMR,[5,6] neutron diffraction,[7] electron microscopy,[13] and scanning tunneling spectroscopy[11] have been done on bulk single crystals or polycrystals to observe the inhomogeneous states. Epitaxial thin films encounter difficulty in precise characterization of such physical properties as magnetism due to the small volume and lattice strain effect caused by the interaction with the substrate. Nevertheless, thin films can offer advantages that are hardly realized in bulk specimens. We can expect artificial control of charge order or phase separation in $R_{1-x}A_x\text{MnO}_3$ by fabrication of the superlattice $[(R\text{MnO}_3)_l/(A\text{MnO}_3)_m]_n$, if the *B*-site valence is dominated by the *A*-site cation valence. Here, we report on parallel fabrication of $[(\text{LaMnO}_3)_m/(\text{SrMnO}_3)_m]_n$ superlattices on $\text{SrTiO}_3(100)$ having different periodicity (m), as well as on elucidation of the effects of *A*-site cation ordering along the growth direction in superlattices on their magnetic and electric properties. The averaged hole concentration in the superlattices was fixed at 0.5, the boundary between the hole doped regime ($x < 0.5$), where the ferromagnetic phases appear, and the electron doped regime ($x > 0.5$), where the antiferromagnetic phases appear. There are reports of manganese perovskite superlattices which focus on the antiferromagnetic/ferromagnetic interaction of the superlattice constituents;[14,15] however, there are few reports on charge inhomogeneity.[16]

II. EXPERIMENT

$[(\text{LaMnO}_3)_m/(\text{SrMnO}_3)_m]_n$ with $(m,n) = (1,96)$, $(2,48)$, $(4,24)$, $(8,12)$, $(16,6)$, and $(32,3)$ and 50 nm thick LaMnO_3 and SrMnO_3 films were fabricated using a combinatorial pulsed laser deposition system, which is schematically illustrated in Figs. 1(a) and 1(b). A pattern mask having a set of five 1.5 mm wide slits was positioned 1 mm beneath the substrate and the shadow mask worked to choose which slits
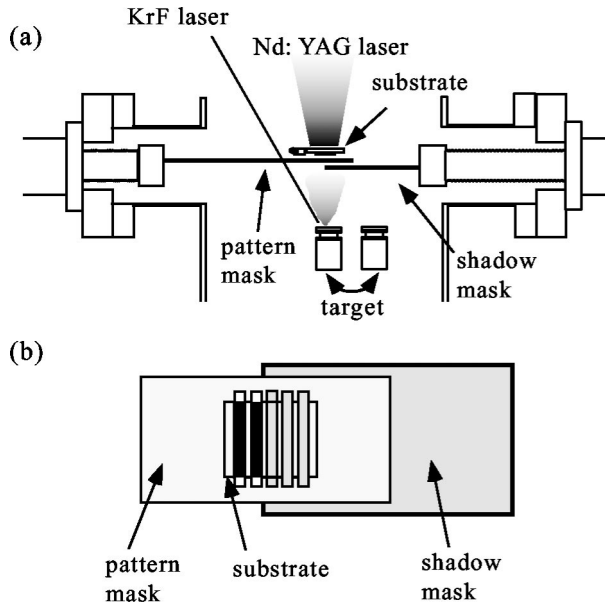
FIG. 1. (a) Combinatorial pulse laser deposition chamber. A pattern mask and a shadow mask are driven by two linear stepping motors. (b) The pattern mask is used for sample pad area definition and the shadow mask is used to choose which slits in the pattern mask are actually open for the deposition (shaded area).

FIG. 2. 2θ-θ x-ray diffraction scans around the (001) fundamental peaks of $[(\mathrm{LaMnO_3})_m/(\mathrm{SrMnO_3})_m]_n$ ($m=1,4,16$) superlattices. The fundamental peaks and satellite peaks caused by A-site cation order are marked by ticks.

in the pattern mask were actually open for the deposition of as many as five different films (1.5×7.5 mm^2) on a substrate heated by a Nd:YAG (yttrium aluminum garnet) (cw) laser. Synchronizing the target exchange with the mask and shutter switching enabled parallel synthesis of five different compositions and/or layer sequence. The details of the thin film growth system were reported elsewhere.[2,17,18] The KrF excimer laser pulses were focused on sintered ceramic LaMnO$_3$ and SrMnO$_3$ targets at a fluence of 5 J/cm^2. The depositions were carried out on buffered NH$_4$F-HF treated SrTiO$_3$(100) substrates[19] having atomically flat terraces and steps with single unit cell height at 800 °C in a 1×10^{-3} Torr oxygen atmosphere. The periodicities of the superlattices were controlled by monitoring the reflection high-energy electron diffraction (RHEED) specular spot intensity oscillations simultaneously at five points on a substrate using a scanning RHEED system.[17,18] After the deposition, the chamber was filled with 1 atm oxygen gas and the sample was cooled to room temperature at a rate of 10°C/min. Another library of $[(\mathrm{La_{0.8}Sr_{0.2}MnO_3})_8/(\mathrm{La_{0.2}Sr_{0.8}MnO_3})_m]_{12}$ with $m=1$, 3, 4,

7, 8, and 50 nm thick La$_{1-x}$Sr$_x$MnO$_3$ ($x=0.2$ and 0.8) films were also fabricated under the same conditions (except for the use of La$_{0.8}$Sr$_{0.2}$MnO$_3$ and La$_{0.2}$Sr$_{0.8}$MnO$_3$ targets). Table I shows the film compositions and sequences of three libraries. The surface morphology was analyzed by an atomic force microscope (AFM). The crystal structure was investigated by x-ray diffraction using a 2θ-θ diffractometer. The magnetic measurements were done by using a superconducting quantum interference device. Magnetoresistance was measured by a conventional four-probe method. For structural, magnetic, and transport measurements of each film, each film was cut in 1.2×7.5 mm^2 size to eliminate the effects of edges.

III. RESULTS AND DISCUSSIONS

A. Structural characterization

Figure 2 shows the x-ray diffraction patterns of three $[(\mathrm{LaMnO_3})_m/(\mathrm{SrMnO_3})_m]_n$ $[(m,n)=(1,96),(4,24),(16,6)]$ superlattices on a single substrate. Clear satellite peaks caused by artificial A-site cation order are observed even in the $m=1$ sample. The superlattice periods of the $m=1$, 4, and 16 samples, determined from the x-ray data, were 0.784,

TABLE I. Film composition and sequences of three libraries (A, B, C). Each library has five different films, which were synthesized in parallel on a single substrate.

chip library	1	2	3	4	5
A	LaMnO$_3$	$[(\mathrm{LaMnO_3})m/(\mathrm{SrMnO_3})m]n$ (1.96)	(4.24)	superlattices (16.6)	SrMnO$_3$
B	LaMnO$_3$	$[(\mathrm{LaMnO_3})m/(\mathrm{SrMnO_3})m]n$ (2.48)	(8.12)	superlattices (32.3)	SrMnO$_3$
C		$[(\mathrm{La_{0.8}Sr_{0.2}MnO_3})_8/(\mathrm{La_{0.2}Sr_{0.8}MnO_3})_m]_{12}$ superlattices			
	$m=1$	$m=3$	$m=4$	$m=7$	$m=8$
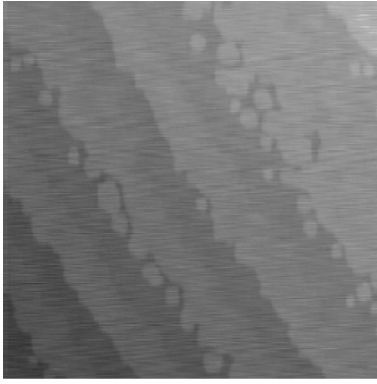
FIG. 3. An AFM image (1000×1000 nm^2) of the $m = 1$ super-lattice. The step height corresponds to the height of a single perov-skite unit cell.

3.06, and 12.5 nm, respectively, in good agreement with the expected values. The mismatches are $+2.1\%$, -0.68%, and $+1.0\%$, respectively. The other superlattices also exhibited satellite peaks consistent with the designed superlattices. An AFM image of the $m = 1$ sample is shown in Fig. 3. Clear steps and atomically flat terraces are visible. These results indicate that an abrupt interface between the SrMnO$_3$ and LaMnO$_3$ layers in the superlattices and the diffusion length of A-site cations at the LaMnO$_3$/SrMnO$_3$ interface is less than 1 unit cell (0.4 nm) of the perovskite structure.

B. Magnetic and electrical properties

Figure 4 shows the magnetization (a), resistivity (b), and magnetoresistance (MR) (c) of LaMnO$_3$, SrMnO$_3$, and $[(\text{LaMnO}_3)_m/(\text{SrMnO}_3)_m]_n$ superlattices as a function of temperature. The LaMnO$_3$ film shows weak magnetization at temperatures below 130 K and insulating behavior below 400 K, while the SrMnO$_3$ film shows negligibly small mag-netization and insulating behavior (over 10^2 Ω cm below 400 K). Stoichiometric LaMnO$_3$ is an A-type (canted) antiferro-magnet (A-AF) below its Néel temperature $T_N = 135$ K, with alternating $d_{3x^2-r^2}/d_{3y^2-r^2}$ orbital ordering with cooperative Jahn-Teller distortion.[20] The observed small magnetization is presumably caused by the La or O deficiency.[21] The cubic perovskite SrMnO$_3$ is a G-type antiferromagnet (G-AF) with $T_N = 260$ K.[22] The superlattices of $m \leq 4$ show relatively small magnetization and metallic behavior below 300 K and large MR at low temperature. This behavior is similar to that of epitaxial La$_{0.5}$Sr$_{0.5}$MnO$_3$ films on SrTiO$_3$(100), which be-haves as an A-type antiferromagnetic metal due to the tensile stress from the substrate.[23,24] With an increase of the super-lattice period from $m = 1$ to 4, increases of magnetization, resistivity, and MR around the onset temperature in M-T curves were observed systematically. On increasing m above 8, drastic changes of magnetic and transport properties oc-curred, i.e., significant suppression of the onset temperature in M-T curves and nonmetallic behavior over the whole tem-perature. With an increase of m from 8 to 32, the resistivity increased systematically, while the magnetization at low tem-perature and the onset temperature slightly decreased.
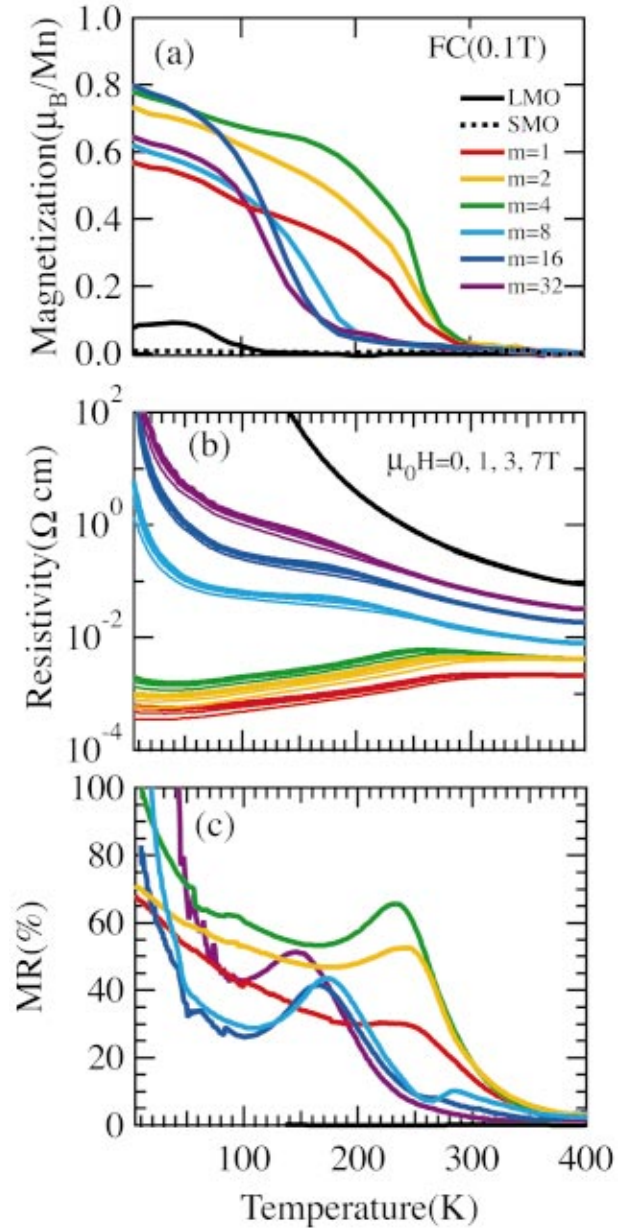
FIG. 4. (Color) (a) Magnetization of nondoped films (LaMnO$_3$, SrMnO$_3$) and $[(\text{LaMnO}_3)_m/(\text{SrMnO}_3)_m]_n$ superlattices ($m = 1,2,4,8,16,32$) as a function of temperature in a field of 0.1 T along the [100] direction in the film plane during a field cooling process. The magnetization data is normalized by the total number of Mn ions in the films. (b) Resistivity of the superlattices and the LaMnO$_3$ film as a function of temperature in a magnetic field (0,1,3,7 T). The thick line shows the resistivity without a magnetic field. The magnetic field was applied parallel to the current, along the [100] direction in the film plane. (c) Negative MR $[\rho(0\ \text{T}) - \rho(7\ \text{T})]/\rho(7T) \times 100)$ of the superlattices and the LaMnO$_3$ film as a function of temperature.

These results indicate that the magnetoelectric properties of the superlattices were determined by magnetic interaction between the superlattice constituents and mixed valence of Mn ions caused by carrier (e_g electrons) transfer thorough the superlattice interface depending on the number of m. The
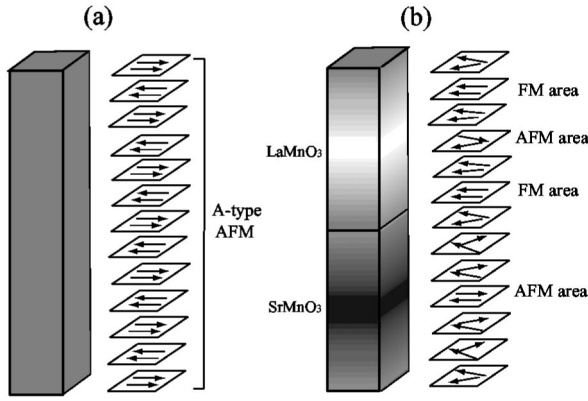
FIG. 5. Schematic illustrations of solid solution $La_{0.5}Sr_{0.5}MnO_3$ (a) and $[(LaMnO_3)_m/(SrMnO_3)_m]_n$ superlattice (b). The color shows the hole concentration of the e_g orbital and the dark region has higher hole concentration than the light region. The arrows show the spin alignment of MnO_2 planes. $La_{0.5}Sr_{0.5}MnO_3$ has relatively homogeneous hole concentration along the growth direction and shows A-type antiferromagnetism, while the superlattice has inhomogeneous hole concentration and magnetic states.

existence of carrier transfer is clearly indicated by the appearance of ferromagnetism in antiferromagnetic $(LaMnO_3)$/ antiferromagnetic $(SrMnO_3)$ superlattices with large m (≥ 8) and the increase of magnetization from $m=1$ to 4. If the Mn ion valence was determined only by the nearest A-site cations, that is, the charge neutrality was preserved

strictly on the one unit cell scale, and the $LaMnO_3$ and $SrMnO_3$ layers preserved their original magnetic properties (A-AF and G-AF), the magnetization of the superlattices should show values between those of $LaMnO_3$ and $SrMnO_3$. If the charge neutrality was preserved on a larger scale and holes are doped into the $LaMnO_3$ layers from the $SrMnO_3$ layers through the interface, ferromagnetism would appear due to ferromagnetic coupling of Mn^{3+} and Mn^{4+}, as seen in divalent-substituted $La_{1-x}Sr_xMnO_3$ $(0.15 \leq x < 0.5)$,[25] lanthanum-deficient $La_xMnO_{3-\delta}$ $(x \leq 1)$,[21] and oxygen-overdoped $LaMnO_{3+\delta}$ $(\delta \geq 0)$.[20] Electrons doped into the $SrMnO_3$ layers would not give rise to ferromagnetism because $La_{1-x}Sr_xMnO_3$ $(x > 0.5)$ is antiferromagnetic.[1] Another potential source of the ferromagnetic response is the magnetization of Mn ions, which is in the interface layers. This effect, however, can also be discarded because in this case we should see the strongest ferromagnetic response in the $m=1$ sample. The magnetization values of all other superlattices should then be between those of $LaMnO_3$ and the $m=1$ sample. This is clearly not the case, as shown in Fig. 4(a). The x-ray and AFM results also showed that A-site cation diffusion at the interfaces is negligible and cannot cause changes in the magnetic structure of the superlattices.

The hole distribution and magnetic states along the growth direction in the solid solution $La_{0.5}Sr_{0.5}MnO_3$ film and superlattices are schematically illustrated in Fig. 5. In the solid solution $La_{0.5}Sr_{0.5}MnO_3$ film, random distribution of A-site cations results in a homogeneous hole distribution in
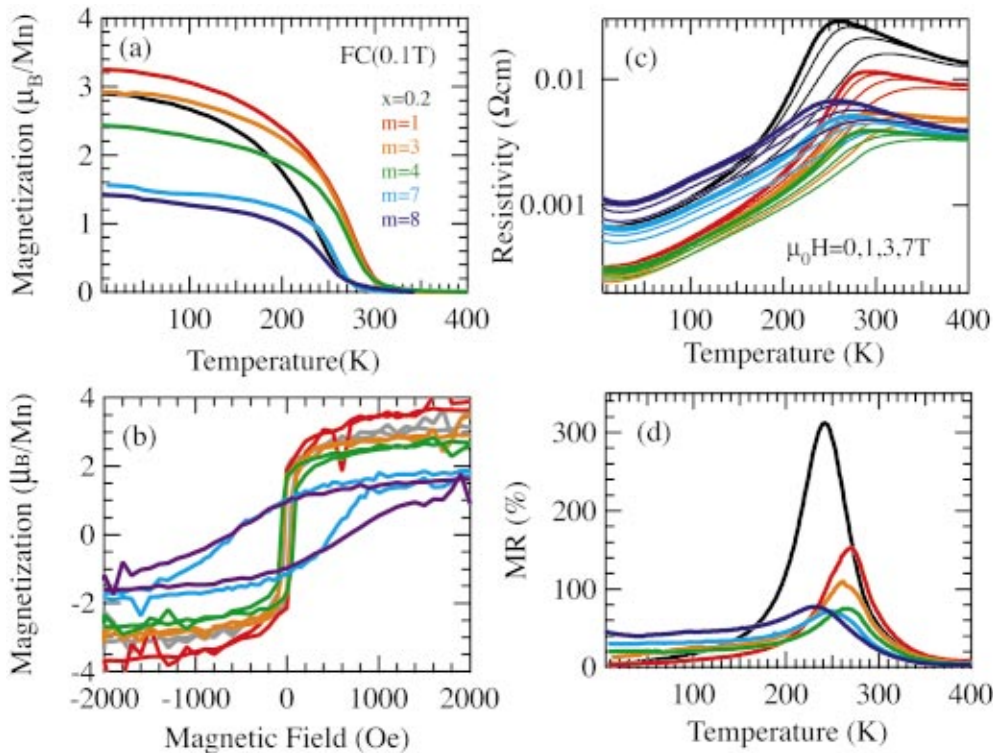
FIG. 6. (Color) (a) Magnetization of $La_{0.8}Sr_{0.2}MnO_3$ film and $[(La_{0.8}Sr_{0.2}MnO_3)_8/(La_{0.2}Sr_{0.8}MnO_3)_m]_{12}$ superlattices ($m=1,3,4,7,8$) as a function of temperature in a field of 0.1 T along the [100] direction in the film plane during a field cooling process. (b) M-H hysteresis curves for the samples at 5 K. (c) Resistivity of the samples as a function of temperature in a magnetic field (0,1,3,7 T). The thick line shows the resistivity without a magnetic field. (d) Negative MR $[\rho(0T)-\rho(7\ T)]/\rho(7\ T)\times 100$ of the samples as a function of temperature.
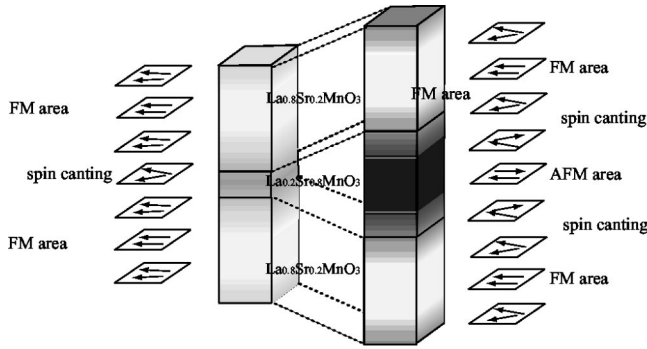
FIG. 7. Schematic illustrations of $[(La_{0.8}Sr_{0.2}MnO_3)_8/(La_{0.2}Sr_{0.8}MnO_3)_m]_{12}$ superlattices. The color shows the hole concentration of e_g orbital and the dark region has higher hole concentration than the light region. The arrows show the spin alignment of MnO_2 planes. A small m superlattice has relatively homogeneous hole concentration and ferromagnetic states along the growth direction due to the carrier transfer through the interface, while a large m superlattice has inhomogeneous hole concentration and magnetic states.

the film and the averaged ionic valence of Mn is 3.5, showing *A*-type antiferromagnetic metal behavior [Fig. 5(a)]. In the case of superlattices, the average ionic valence of Mn at the interface is 3.5; therefore, all of the Mn ions in the $m=1$ sample are equivalent, which is the same situation as in solid solution $La_{0.5}Sr_{0.5}MnO_3$. In $m\leqslant 4$ samples, the modulation amplitude and period of hole concentration will be small due to the small m value and charge transfer at $LaMnO_3/SrMnO_3$ interfaces. The observed properties are therefore similar to those of a solid solution $La_{0.5}Sr_{0.5}MnO_3$ film. The slight increases of magnetization, resistivity, and MR around the onset temperature in *M*-*T* indicate that the system gradually evolves as m increases from a hole concentration and magnetic structure distribution that are both nearly homogeneous and resemble those of a solid solution film to those of structures which show clear modulation along the superlattice growth direction. On the other hand, in $m\geqslant 8$ samples, the modulation amplitude and period will be large and we have a form of artificially generated phase separation in the sample. The $SrMnO_3$ layers retain their antiferromagnetic character, while the $LaMnO_3$ layers, particularly close to the interfaces, are ferromagnetic as shown in Fig. 5(b). These differences in hole concentration and magnetic structure distribution result in the large difference in magnetic and transport properties between the $m\leqslant 4$ and $m\geqslant 8$ samples.

Other clear indications of magnetic interactions and charge transfer between the superlattice constituents have been provided from the magnetic and electric properties of $[(La_{0.8}Sr_{0.2}MnO_3)_8/(La_{0.2}Sr_{0.8}MnO_3)_m]_{12}$ ($m=1,3,4,7,8$) superlattices, where $La_{0.8}Sr_{0.2}MnO_3$ is a ferromagnetic metal and $La_{0.2}Sr_{0.8}MnO_3$ is an antiferromagnetic insulator.[2] In this case, the effects of magnetic interactions between the superlattice constituents can be evaluated because the thickness of each $La_{0.8}Sr_{0.2}MnO_3$ layer was fixed, whereas that of the $La_{0.2}Sr_{0.8}MnO_3$ layer was varied systematically. Figure 6 shows the temperature dependences of magnetization (a), re-
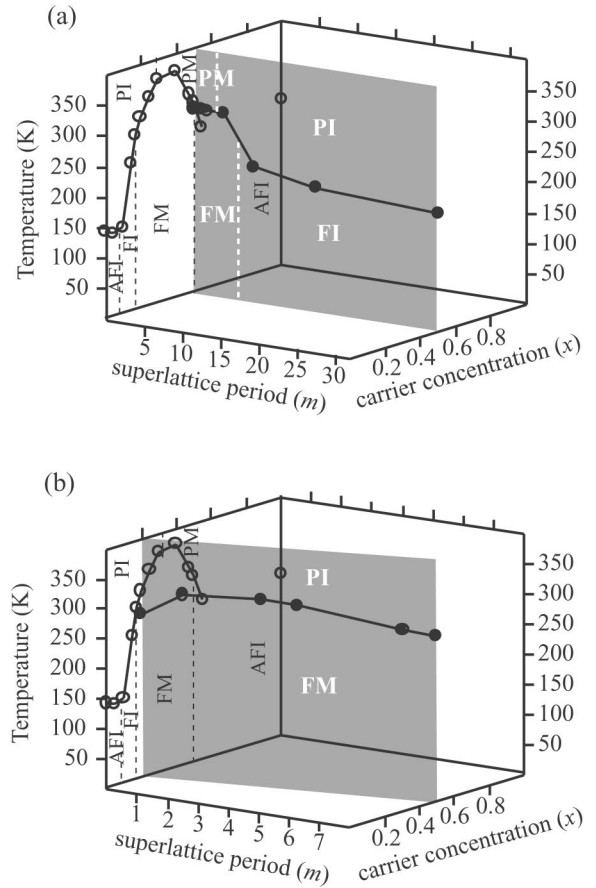
FIG. 8. Magnetic and electrical phase diagrams of the $[(LaMnO_3)_m/(SrMnO_3)_m]_n$ (a) and $[(La_{0.8}Sr_{0.2}MnO_3)_8/(La_{0.2}Sr_{0.8}MnO_3)_m]_{12}$ (b) superlattices as functions of superlattice periodicity and averaged hole concentration (x) in the superlattices and those of solid solution $La_{1-x}Sr_xMnO_3$ bulk samples. The phase diagrams of the superlattices correspond to the shaded planes and those of solid solution samples correspond to the $m=0$ planes. PI; paramagnetic insulator, PM; paramagnetic metal, AFI; antiferromagnetic insulator, FI; ferromagnetic insulator, and FM, ferromagnetic metal.

sistivity (c), and MR (d) as well as the *M*-*H* curves (b) at 5 K of the superlattices and the $La_{0.8}Sr_{0.2}MnO_3$ film as a reference. In spite of the substitution of antiferromagnetic insulating $La_{0.2}Sr_{0.8}MnO_3$ layers for ferromagnetic metal $La_{0.8}Sr_{0.2}MnO_3$ layers in the superlattices, the $m\leqslant 4$ samples show larger onset temperature in *M*-*T* curves and lower resistivity than $La_{0.8}Sr_{0.2}MnO_3$ films. The superlattices maintain soft magnetism with a coercive field below 100 Oe, just like $La_{0.8}Sr_{0.2}MnO_3$. On the other hand, the superlattices of $m\geqslant 7$ show hard magnetism with a coercive field over 500 Oe. Also observed are strong suppression of the onset temperature and saturated magnetization, and increase of resistivity and MR at low temperature.

Figure 7 shows the schematic illustration of hole distribution and magnetic states along the growth direction in the superlattices. When m is below 4, some holes are transferred from $La_{0.2}Sr_{0.8}MnO_3$ to $La_{0.8}Sr_{0.2}MnO_3$ layers and the hole concentration will become relatively homogeneous along the growth direction of the superlattice. Therefore the superlat-

tice exhibits onset temperature and conductivity higher than the solid solution $La_{0.8}Sr_{0.2}MnO_3$ film. When m is over 7, the hole concentration will become inhomogeneous and phase separation will occur along the growth direction. Thus, the superlattice has a property deviating from that of the solid solution: reduced ferromagnetic metal states with high coercive field due to the magnetic coupling between the superlattice constituents.

Figure 8 summarizes the magnetic and electrical phase diagram of the fabricated $[(LaMnO_3)_m/(SrMnO_3)_m]_n$ superlattices (a) and $[(La_{0.8}Sr_{0.2}MnO_3)_8/(La_{0.2}Sr_{0.8}MnO_3)_m]_{12}$ superlattices (b) as functions of superlattice periodicity (m) and averaged hole concentration (x) as compared with the diagram of the solid solution $La_{1-x}Sr_xMnO_3$ bulk sample ($m=0$). As discussed above, the electrical and magnetic states of the superlattices were strongly dependent on the periodicity and there was a critical number dividing the solid-solution-like properties and the properties that deviated from those of the solid solution. There should be several physical reasons for the existence of the critical number in these superlattices. The possible contributions are Coulomb interaction to maintain charge neutrality, exchange interaction between the neighboring Mn ions, and the kinetic energy of the e_g electrons. Therefore, the critical number depends on the combination of superlattice constituents. In the case of $[(LaMnO_3)_m/(SrMnO_3)_m]_n$ and $[(La_{0.8}Sr_{0.2}MnO_3)_8/(La_{0.2}Sr_{0.8}MnO_3)_m]_{12}$ superlattices, the critical number was between 4 and 8. The A-site cation ordering, which enables one to change both the effective carrier concentration and magnetic interaction, is an important parameter for controlling the material properties.

IV. CONCLUSION

We have fabricated epitaxial $[(LaMnO_3)_m/(SrMnO_3)_m]_n$ superlattices on $SrTiO_3(100)$ by the combinatorial pulsed laser deposition method to investigate the effect of A-site cation ordering on the magnetic and electric properties. The properties of superlattices were found to depend strongly on the periodicity m. The superlattices of $m\leq4$ behaved like solid solution $La_{0.5}Sr_{0.5}MnO_3$, with metallic behavior and small magnetization below 300 K, while the superlattices of $m>4$ deviated from the behavior of a solid solution, showing nonmetallic behavior and significant suppression of the Curie temperature compared to those of superlattices of $m\leq4$. These results indicate that the properties of the superlattices are dominated not only by the magnetic interaction between the superlattice constituents but also by the carrier (e_g electrons) transfer thorough the superlattice interface. Their contributions are also supported by the magnetoelectric properties of other $[(La_{0.8}Sr_{0.2}MnO_3)_8/(La_{0.2}Sr_{0.8}MnO_3)_m]_{12}$ superlattices. The A-site cation ordering enables us to change both the effective carrier concentration and the magnetic interaction; therefore, it provides us with an opportunity to fabricate artificial lattices with desired properties (electrical, magnetic, and magnetoresistive properties) or innovative electromagnetic properties.

[1] For example, M. Imada, A. Fujimori, and Y. Tokura, Rev. Mod. Phys. **70**, 1039 (1998).

[2] T. Fukumura, Y. Okimoto, M. Ohtani, T. Kageyama, T. Koida, M. Kawasaki, T. Hasegawa, Y. Tokura, and H. Koinuma, Appl. Phys. Lett. **77**, 3426 (2000).

[3] P.W. Anderson and H. Hasegawa, Phys. Rev. **100**, 675 (1955).

[4] A.J. Millis, P.B. Littlewood, and B.I. Shraiman, Phys. Rev. Lett. **74**, 5144 (1995).

[5] G. Allodi, R. De Renzi, and G. Guidi, Phys. Rev. B **57**, 1024 (1998).

[6] G. Papavassiliou, M. Fardis, F. Milia, A. Simopoulos, G. Kallias, D. Niarchos, and N. Ioannidis, Phys. Rev. B **55**, 15 000 (1997).

[7] M.R. Ibarra, Guo-meng Zhao, J.M. De Teresa, B. Garcia-Landa, Z. Arnold, C. Marquina, P.A. Algarabel, H. Keller, and C. Ritter, Phys. Rev. B **57**, 7446 (1998).

[8] H. Fujishiro, M. Ikebe, and Y. Konno, J. Phys. Soc. Jpn. **67**, 1799 (1998).

[9] S.I. Patil *et al.*, Phys. Rev. B **62**, 9548 (2000).

[10] K.H. Kim, J.H. Jung, and T.W. Noh, Phys. Rev. Lett. **81**, 1517 (1998).

[11] M. Fath, S. Fresem, A.A. Menovsky, Y. Tomioka, L. Aarts, and J.A. Mydosh, Science **285**, 1540 (1999).

[12] A. Moreo, S. Yunoki, and E. Dagotto, Science **283**, 2034 (1999).

[13] M. Uehara, S. Mori, C.H. Chen, and S.W. Cheong, Nature (London) **399**, 560 (1999).

[14] H. Tanaka and T. Kawai, Solid State Commun. **112**, 201 (1999).

[15] M. Izumi, T. Manako, Y. Konishi, M. Kawasaki, and Y. Tokura, Phys. Rev. B **61**, 12 187 (2000).

[16] P.A. Salvador, A.-M. Haghiri-Gosnet, B. Mercey, M. Hervieu, and B. Raveau, Appl. Phys. Lett. **75**, 2638 (1999).

[17] H. Koinuma, T. Koida, T. Ohnishi, D. Komiyama, M. Lippmaa, and M. Kawasaki, Appl. Phys. A: Mater. Sci. Process. **69**, s29 (1999).

[18] T. Ohnishi, D. Komiyama, T. Koida, S. Ohashi, C. Stauter, H. Koinuma, A. Ohtomo, M. Lippmaa, N. Nakagawa, M. Kawasaki, T. Kikuchi, and K. Omote, Appl. Phys. Lett. **79**, 536 (2001).

[19] M. Kawasaki, K. Takahashi, T. Maeda, R. Tsuchiya, M. Shinohara, T. Yonezawa, O. Ishihara, M. Yoshimoto, and H. Koinuma, Science **266**, 1540 (1994).

[20] J. Topfer and J.B. Goodenough, J. Solid State Chem. **130**, 117 (1997).

[21] A. Gupta, T.R. McGuire, P.R. Duncombe, M. Rupp, J.Z. Sun, W.J. Gallagher, and G. Xiao, Appl. Phys. Lett. **67**, 3494 (1995).

[22] T. Takeda and S. Ohara, J. Phys. Soc. Jpn. **37**, 275 (1974).

[23] Y. Konishi, Z. Fang, M. Izumi, T. Manako, T. Kasai, H. Kuwahara, M. Kawasaki, K. Terakura, and Y. Tokura, J. Phys. Soc. Jpn. **68**, 3790 (1999).

[24] T. Koida, D. Komiyama, H. Koinuma, M. Ohtani, M. Lippmaa, and M. Kawasaki, Appl. Phys. Lett. **80**, 565 (2002).

[25] A. Urushibara, Y. Morimoto, T. Arima, A. Asamitsu, G. Kido, and Y. Tokura, Phys. Rev. B **51**, 14 103 (1995).